Self-Assembled Monolayers of 6-Phenyl-n-hexanethiol and 6-(p-Vinylphenyl)-n-hexanethiol on Au (111): An Investigation of Structure, Stability, and Reactivity

ARTICLE *in* LANGMUIR · MAY 2001

Impact Factor: 4.46 · DOI: 10.1021/la001633u

Self-Assembled Monolayers of 6-Phenyl-*n*-hexanethiol and 6-(*p*-Vinylphenyl)-*n*-hexanethiol on Au(111): An Investigation of Structure, Stability, and Reactivity

Lili Duan and Simon J. Garrett*

Department of Chemistry, Michigan State University, East Lansing, Michigan 48824

Received November 27, 2000. In Final Form: February 22, 2001

Self-assembled monolayers (SAMs) of 6-phenyl-*n*-hexanethiol (PHT) and 6-(*p*-vinylphenyl)-*n*-hexanethiol (VHT) on Au(111) have been investigated by reflection−absorption infrared spectroscopy (RAIRS), ellipsometry, and scanning tunneling microscopy (STM). Both molecules chemisorbed as thiolates. The packing order and structural changes of the PHT monolayer were investigated at room temperature and following annealing in ultrahigh vacuum. Three different stripe phases (δ, χ', and β), characterized by molecular axes oriented almost parallel to the surface plane, were observed by STM. In contrast, the VHT monolayer had a structure in which the average molecular tilt angle was close to the surface normal. Polymerization of the VHT SAM, as followed by RAIRS, was achieved by either UV-light irradiation or thermal treatment. Ultraviolet irradiation produced longer chain polymers with a maximum of ∼70% conversion, whereas annealing produced shorter chain polymers with CH_3 as the end group. The UV-light polymerized film was more robust than the thermally polymerized film.

1. Introduction

Self-assembled monolayers (SAMs) have received a great deal of attention because of their fundamental importance in understanding interfacial properties and for their potential application in molecular-based technologies.[1,2] One of the most popular systems has been monolayers of ω-substituted thiols of the form HS−$(CH_2)_n$−X chemisorbed on Au(111). Such substituted SAMs modify both the chemical and physical properties of the substrate surfaces to which they bond and can be used to provide a variety of chemically tailored surfaces. Moreover, it has long been recognized that the ω-terminus can provide a convenient attachment point for subsequent chemistry. In this way, derivatized surfaces or multilayer assemblies may be produced.

The dependence of the monolayer morphology on the chemical nature of the end group has been studied for a range of terminal groups including X = CH_3, COOH, CH=CH_2, CF_3, OH, and $NH_3^+Cl^-$.[3−12] The first three end groups result in similar hexagonal ($\sqrt{3}\times\sqrt{3}$)R30°-based structures, whereas CF_3-terminated SAMs show only short-range order. Both OH- and $NH_3^+Cl^-$-terminated SAMs adopt unique packing structures, which are fundamentally different from the hexagonal lattice. It can be concluded that in addition to surface−adsorbate interactions, the packing arrangement of ω-substituted thiols is influenced by the interactions between both alkyl chains and end groups. We are interested in studying alkanethiol SAMs terminated by aromatic groups. The aromatic group is much less flexible than an alkyl chain, and the dominant interactions between aromatic moieties may include face-to-face or edge-to-face π-bonding contributions in addition to the simple van der Waals forces believed to dominate the packing of alkyl chains.[13−15] Furthermore, the presence of a bulky aromatic group may sterically prevent the formation of the well-documented ($\sqrt{3}\times\sqrt{3}$)R30° close-packed monolayer structure.

Azobenzene derivatives have been studied as model SAMs in order to determine the magnitudes of the aromatic and aliphatic interactions and their effect on monolayer structure.[16−20] In general, the alkyl portions of the chains are somewhat disordered, and the packing is dominated by attractive interactions between the aromatic portions of the molecules. Interestingly, minor molecular modification produces major differences in the morphologies of the SAM, suggesting that in these systems there is a delicate balance between aromatic, aliphatic, and substrate interactions.

* To whom correspondence should be addressed. Phone: (517)-355-9715 ext. 208. Fax: (517)353-1793. E-mail: garrett@cem.msu.edu.

(1) Ulman, A. *An Introduction to Ultrathin Organic Films from Langmuir−Blodgett to Self-Assembly*; Academic Press: San Diego, CA, 1991.
(2) Whitesides, G. M.; Gorman, C. B. In *The Handbook of Surface Imaging and Visualization*; Hubbard, A. T., Ed.; CRC Press: Boca Raton, FL, 1995; p 713.
(3) Nuzzo, R. G.; Fusco, F. A.; Allara, D. L. *J. Am. Chem. Soc.* **1987**, *109*, 2358.
(4) Nuzzo, R. G.; Dubois, L. H.; Allara, D. L. *J. Am. Chem. Soc.* **1990**, *112*, 558.
(5) Leung, T. Y. B. Ph.D. Thesis, Princeton University, Princeton, NJ, 1998.
(6) Li, J.; Liang, K. S.; Scoles, G.; Ulman, A. *Langmuir* **1995**, *11*, 4418.
(7) Hutt, D. A.; Leggett, G. J. *Langmuir* **1997**, *13*, 2740.
(8) Yan, L.; Marzolin, C.; Terfort, A.; Whitesides, G. M. *Langmuir* **1997**, *13*, 6704.
(9) Boubour, E.; Lennox, R. B. *Langmuir* **2000**, *16*, 7464.
(10) Poirier, G. E.; Pylant, E. D.; White, J. M. *J. Chem. Phys.* **1996**, *105*, 2089.
(11) Pfaum, J.; Bracco, G.; Scoles, G.; Lee, R.; Kahn, A. *Am. Vac. Soc. Int. Symp. Abstr.* **2000**, 55.
(12) Kawasaki, M.; Sato, T.; Yoshimoto, T. *Langmuir* **2000**, *16*, 5409.
(13) Whitten, D. G.; Chen, L.; Geiger, C.; Perlstein, J.; Song, X. *J. Phys. Chem. B* **1998**, *102*, 10098.
(14) Song, X.; Geiger, H. C.; Farahat, M.; Perlstein, J.; Whitten, D. G. *J. Am. Chem. Soc.* **1997**, *119*, 12481.
(15) Vadey, S.; Deiger, H. C.; Cleary, B.; Perlstein, J.; Whitten, D. G. *J. Phys. Chem. B* **1997**, *101*, 321.
(16) Caldwell, W. B.; Csmpbell, D. J.; Chen, K.; Herr, B. R.; Mirkin, C. A.; Malik, A.; Durbin, M. K.; Dutta, P.; Huang, K. G. *J. Am. Chem. Soc.* **1995**, *117*, 6071.
(17) Wang, R.; Iyoda, T.; Jiang, L.; Hashimoto, K.; Fujishima, A. *Chem. Lett.* **1996**, 1005.
(18) Tamada, K.; Nagasawa, J.; Nakanishi, F.; Abe, K.; Ishita, T.; Hara, M.; Knoll, W. *Langmuir* **1998**, *14*, 3264.
(19) Han, S. W.; Kim, C. H.; Hong, S. H.; Chung, Y. K.; Kim, K. *Langmuir* **1999**, *15*, 1579.
(20) Yu, H. Z.; Ye, S.; Zhang, H. L.; Uosaki, K.; Liu, Z. F. *Langmuir* **2000**, *16*, 6948.

10.1021/la001633u CCC: $20.00
Published on Web 04/03/2001

Simple alkanethiols can form dense, well-packed monolayers on some metal surfaces; however, a serious deficiency for practical applications is their thermal and mechanical fragility. The incorporation of unsaturation into the SAM provides the opportunity for subsequent chemistry either through attachment of another species or by intralayer cross-linking reactions (oligomerization/polymerization). Increasing the lateral interaction between the chains by covalent bonding can improve the robustness of the SAMs.[21] After spontaneous assembly of thiols onto a gold substrate, cross-linking of adjacent molecules can be initiated by chemical, photo, or thermal means. However, in highly ordered monolayers, such as SAMs, geometric structure, molecular motion, and diffusion are likely to play important roles in determining reaction probability and specificity. As in solid state polymerization, structural control of potential reaction geometry is expected, and in appropriately organized systems, there may be minimal disruption of the monolayer structure by the interconnection process. In principle, polymerization reactions in SAMs can be used to produce crystalline macromolecular thin films.

There have been previous studies of photoinduced polymerization of adsorbed monomers on metal surfaces. Ford et al. formed polymerizable monolayers by adsorbing 4-(mercaptomethyl)styrene on a roughened silver surface.[22] The orientation of the benzene ring plane in the styrene moiety was deduced from band intensities in surface-enhanced Raman spectroscopy (SERS) to be slightly inclined from the surface normal. Subsequently, 514 nm laser light was used to both initiate and probe photoreactivity through SERS, and a polymerization reaction was observed. Peanasky and McCarley have studied undec-10-ene-1-thiol/Au SAMs irradiated by γ-rays.[23] The polymerization of the monolayers during γ-ray exposures was indicated by the decrease in the intensities of the infrared bands associated with the olefin functionality. Some disordering of the monolayer occurred during the reaction. It was proposed that the polymerization reaction was controlled by the distance that the tethered olefin groups were able to move. Several groups have studied UV irradiation of self-assembled monolayers containing diacetylene units.[24−28] The incorporation of conjugated diacetylene groups within thiol or disulfide compounds has permitted the fabrication of robust monolayer polymers that are more durable and better barriers to electron transfer than the unpolymerized monolayers. It was suggested that the diacetylene groups were able to undergo topochemical (structure-controlled) reaction in these monolayers.

In this paper, we present our study of phenyl- and styrene-terminated hexanethiol SAMs on Au(111). The phenyl-terminated molecule was used to examine the influence of a simple aromatic terminus on monolayer packing order. The addition of an alkene to the phenyl group (to produce a styrene-terminated SAM) allowed us to study the thermal stability and photopolymerization processes. In both cases, the monolayer thickness and the molecular orientation were determined by ellipsometry and reflection−absorption infrared spectroscopy (RAIRS), respectively. Film morphologies were characterized by scanning tunneling microscopy (STM). Chemical and structural changes induced by thermal or UV irradiation of the SAMs were followed by RAIRS.

2. Experimental Section

2.1. Synthesis. The synthesis of 6-(*p*-vinylphenyl)-*n*-hexanethiol (VHT) was carried out by sequential alkylation and thiolization reactions as follows: (4-Vinylphenyl)magnesium bromide was prepared from 4-bromostyrene (2.32 g, 12.7 mmol) and magnesium metal turnings activated with a few crystals of I_2 in 30 mL of dry tetrahydrofuran (THF).[29] Once the reaction was initiated, dry ice cooling was applied to minimize potential polymerization. This Grignard solution was added to a solution of 1,6-dibromohexane (2.78 g, 11.4 mmol) and Li_2CuCl_4 (0.184 g, 0.72 mmol) in 30 mL of THF.[30] The reaction temperature was kept at 0 °C in an ice−water bath for 20 min and then allowed to warm to room temperature. After 3 h, the reaction mixture was filtered through silica gel and the solvent was removed under reduced pressure. The crude product was purified by silica gel chromatography. 4-(6-Bromohexyl)styrene was obtained as an oily product at 36% yield. Next, to a dried and argon-filled Shlenk flask, sodium bisulfide dihydrate (0.92 g, 9.99 mmol) and the solution of 4-(6-bromohexyl)styrene (0.89 g, 3.33 mmol) in 50 mL of acetone were added. The reaction mixture was stirred at room temperature for 6 h and then filtered through silica gel. Solvent was removed under reduced pressure without air exposure. The flask containing an oily residue was moved into a drybox filled with helium. The crude product was separated on a silica gel column (28 × 2.3 cm, 230−400 mesh) using hexane−chloroform (2:1) giving VHT as a clear oil in 45% yield. The structure of VHT was confirmed from ^{1}H NMR spectra taken in $CDCl_3$ media; δ values were δ 7.35−7.05 (2d, aryl 4H), 6.66 (quartet, vinyl 1H), 5.75−5.15 (2d, vinyl 2H), 2.57 (t, 2H), 2.49 (quartet, 2H), 1.65−1.52 (m, 4H), and 1.44−1.27 (m, 4H + SH). 6-Phenyl-*n*-hexanethiol (PHT) was synthesized in 84% yield from 1-bromo-6-phenylhexane (Lancaster Synthesis Inc.) under the same thiolization reaction condition as described above. Purity was confirmed by ^{1}H NMR and GC−MS.

2.2. Substrate and Monolayer Preparation. The gold substrates for infrared spectroscopy and ellipsometry measurements were made by electron-beam evaporation of 200 nm of Au on 20 nm of Ti on Si(100) wafers. The gold substrates for STM measurements were prepared by thermally evaporating gold onto freshly cleaved mica in high vacuum. In both cases, STM revealed the clean surfaces to be composed of Au grains with (111)-textured terraces (1000−2500 Å) separated by monatomic steps. All of the substrates were cleaned by a UV/O_3 cleaner for 15 min, followed by soaking in deionized water for 30 min. After this, the substrates were dried in flowing N_2 and immediately transferred into a N_2-filled glovebag where they were immersed in 2 mM CH_2Cl_2 solutions of the adsorbates for more than 5 h. The resultant SAMs were sonicated in CH_2Cl_2 to remove excess adsorbate from the surface and dried in a N_2 stream before characterization.

2.3. Infrared Measurements. RAIRS was performed using a N_2-purged Nicolet 560 Magna IR spectrometer with MCT detector. Spectra were obtained with a PIKE specular reflectance accessory using *p*-polarized light incident at 80° with respect to the surface normal. All spectra reported are the average of 256 scans obtained at a resolution of 4 cm^{-1} and referenced against a freshly prepared, clean gold film. Transmission spectra of the pure compounds were recorded on a Mattson 3000 Galaxy Series Fourier transform infrared (FTIR) spectrometer. A drop of the neat liquid was placed between two salt plates, and spectra were obtained at 2 cm^{-1} resolution.

(21) Kim, T.; Chan, K. C.; Crooks, R. M. *J. Am. Chem. Soc.* **1997**, *119*, 189.
(22) Ford, J. F.; Vickers, T. J.; Mann, C. K.; Schlenoff, J. B. *Langmuir* **1996**, *12*, 1944.
(23) Peanasky, J. S.; McCarley, R. L. *Langmuir* **1998**, *14*, 113.
(24) Mowery, M. D.; Kopta, S.; Ogletree, D. F.; Salmeron, M.; Evans, C. E. *Langmuir* **1999**, *15*, 5118.
(25) Cai, M.; Mowery, M. D.; Menzel, H.; Evans, C. E. *Langmuir* **1999**, *15*, 1215.
(26) Menzel, H.; Mowery, M. D.; Cai, M.; Evans, C. E. *J. Phys. Chem. B* **1998**, *102*, 9550.
(27) Kim, T.; Ye, Q.; Sun, L.; Chan, K. C.; Crooks, R. M. *Langmuir* **1996**, *12*, 6065.
(28) Chan, K. C.; Kim, T.; Schoer, J. K.; Crooks, R. M. *J. Am. Chem. Soc.* **1995**, *117*, 5875.
(29) Sekiya, A.; Stille, J. K. *J. Am. Chem. Soc.* **1981**, *103*, 5096.
(30) Burns, D. H.; Miller, J. D.; Chan, H. K.; Delaney, M. O. *J. Am. Chem. Soc.* **1997**, *119*, 2125.

2.4. Ellipsometry. Ellipsometric measurements were made on a rotating analyzer ellipsometer (J. A. Woollam, model M-44) using a white light source and an incidence angle of 75° from the surface normal. The thickness values were determined using 44 wavelengths between 414 and 736 nm. Because the solution of the ellipsometry equation, that is, refractive index versus thickness, could not be obtained simultaneously, a refractive index of 1.5 was assumed for the SAMs. At least six different sampling points were considered in order to obtain an average thickness value.

2.5. STM Measurements. All STM images were obtained in ultrahigh vacuum (UHV) ($<1 \times 10^{-9}$ Torr) using a RHK Technology model UHV-300 scanning tunneling microscope. The STM tips were mechanically cut $Pt_{0.8}Ir_{0.2}$ wires. The STM images were obtained in constant current mode with a typical tunneling current of 80 pA and a bias voltage of +500 mV applied to the sample.

2.6. Polymerization. Prepared VHT monolayers were either photopolymerized or thermally polymerized. For photopolymerization, the SAMs were soaked in pure CH_2Cl_2 in UV-transparent vials mounted 30 mm from a low-pressure Hg lamp ($\lambda \sim 250-400$ nm). The average power density at this distance was 4.5 mW/cm^2 (all lines). Thermal polymerization was carried out by controlled heating in a N_2-purged chamber.

3. Results and Discussion

3.1. Ellipsometry Measurements. Optical ellipsometry was used to determine the average thickness of the various films. After soaking for >5 h, the measured thicknesses of the PHT and VHT SAMs were 6 ± 2 and 14 ± 2 Å, respectively. These results were obtained reproducibly on multiple samples. Molecular mechanics calculations[31] were used to calculate the minimized geometry for PHT and VHT, and in both cases, the plane of the phenyl ring was approximately orthogonal to the plane of the all-trans methylene chains. On the basis of these calculations, the distance from the gold surface to the ω-terminal hydrogen was estimated to be 14.2 Å for PHT and 16.3 Å for VHT. This immediately indicated that in the PHT SAM, the molecules were inclined with an apparent average tilt angle of about 65° from the surface normal. It should be noted that this tilt angle is misleading because STM data (discussed below) revealed that PHT molecules formed a complex monolayer structure. In contrast, the SAM thickness values obtained for VHT indicated a more perpendicular molecular orientation (tilt angle of ~30°, similar to alkanethiols[32]) with respect to the underlying Au(111) surface plane. The surprisingly large difference between PHT and VHT molecular orientations suggested that the vinyl group attached to the para position of the benzene ring in VHT contributed significantly to the interchain interactions in these SAMs.

3.2. IR Measurements. Parts B and D of Figure 1 show the RAIR spectra of VHT and PHT monolayers after extended (>8 h) self-assembly on gold, respectively. For comparison, the neat VHT and PHT liquids' infrared spectra are shown in Figure 1A,C. All peaks in these spectra can be assigned by consulting the data in the literature,[33−35] and the results are summarized in Table 1.

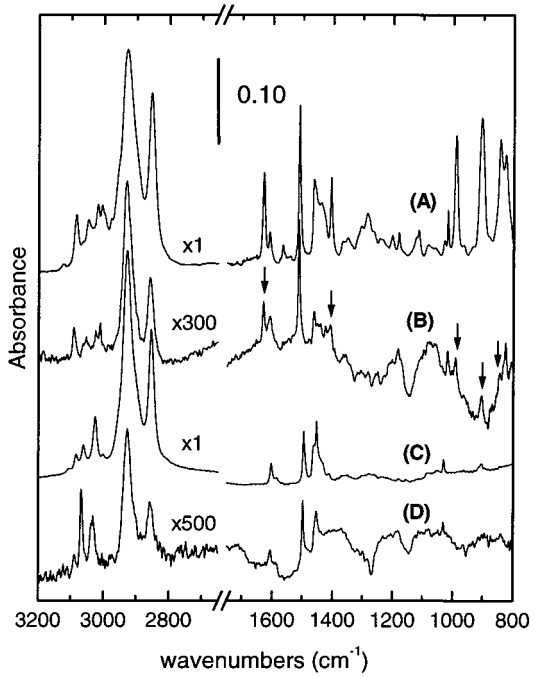

Figure 1. IR spectra of (A) neat VHT, (B) VHT monolayer on a Au/Si wafer, (C) neat PHT, and (D) PHT monolayer on a Au/Si wafer. The arrows indicate the sharp intensity drop of the νC=C, δ=CH$_2$, ω=CH−, ω=CH$_2$, and benzene ring 17b modes, respectively, for the VHT monolayer.

Table 1. Infrared Band Assignments for PHT and VHT[a]

wavenumbers (cm^{-1})					
PHT neat liquid	PHT/Au SAM	VHT neat liquid	VHT/Au SAM	assignment	Wilson's notation
		3084	3089	ν_{as}=CH$_2$	
3084	3088	3047	3051	νCH(arom)	20a
3061	3068				2
3025	3032	3018	3020		20b
		3006	3009	ν=CH−	
		2977	2981	ν_s=CH$_2$	
2928	2927	2928	2928	ν_{as}CH$_2$	
2855	2857	2855	2856	ν_sCH$_2$	
		1629	1630	νC=C	
1604	1606	1609	1608	νCC(ring stretch)	8a
1584	o	o	o		8b
1496	1498	1511	1511		19a
1453	1450	o	1422		19b
1465	1465	1463	1461	δCH$_2$	
		1407	1409	δ=CH$_2$	
1030	1032	1017	1018	δCH(arom)	18a
		990	990	ω=CH−	
		905	905	ω=CH$_2$	
		844	844	ωCH(arom)	17b
		826	826	νCC(arom)	1

[a] o, overlapped band; ν, stretching vibration; δ, in-plane vibration; ω, out-of-plane vibration.

The RAIR spectra taken from films prepared by a 30 min self-assembly were almost identical to those taken from films prepared by up to 24 h self-assembly. This suggests that in common with conventional alkanethiols, a rapid initial adsorption occurred for these mixed aromatic/aliphatic thiols. A weak νS−H feature observed at 2572 cm^{-1} in the liquid RAIR spectra but not in the monolayer spectra confirmed that both PHT and VHT dissociatively chemisorbed as thiolates.

Modes Associated with the Methylene Backbone. It is well-known that the peak positions of the symmetric and the asymmetric CH_2 stretching vibrations can be used as a sensitive indicator of the alkyl chain ordering.[3,32] Lower

(31) Molecular mechanics calculations were performed with SPARTAN 5.0 molecular modeling program (Wavefunction Inc., CA), using empirically based Merck force fields.

(32) Porter, M. D.; Bright, T. B.; Allara, D. L.; Chidsey, C. E. D. *J. Am. Chem. Soc.* **1987**, *109*, 3559.

(33) Colthup, N. B.; Daly, L. H.; Wiberley, S. E. *Introduction to Infrared and Raman Spectroscopy*; Academic Press: Boston, 1990.

(34) Varsanyi, G. *Vibrational Spectra of Benzene Derivatives*; Academic Press: New York and London, 1969.

(35) Varsanyi, G. *Assignments for Vibrational Spectra of Seven Hundred Benzene Derivatives*; John Wiley and Sons: New York, 1974; Vol. 1.

wavenumbers indicate highly ordered conformations with preferential all-trans characteristics (pseudo-crystalline), and for well-ordered alkanethiol SAMs, the $\nu_s CH_2$ and $\nu_{as} CH_2$ modes are usually observed below 2850 and 2920 cm^{-1}, respectively. As shown in Figure 1, the $\nu_s CH_2$ and $\nu_{as} CH_2$ modes for PHT and VHT neat liquids were observed at 2855 and 2928 cm^{-1}, respectively. Upon monolayer formation, although there was some narrowing of these bands, they remained almost completely unshifted with respect to the liquid phase (at $\nu_s CH_2 \sim 2857$ cm^{-1} and $\nu_{as} CH_2 \sim 2927$ cm^{-1}). This implies that in the adsorbed state on Au(111), the aliphatic chains for PHT and VHT were disordered (liquidlike), in marked contrast to alkanethiols with similar overall molecular length (octanethiol) on Au(111).

Modes Associated with the Phenyl Ring. There are five infrared-active aromatic C−H modes in the 3100−3000 cm^{-1} region: 20a, 2, 7b, 20b, and 7a modes in approximate order of decreasing wavenumber.[34] Of these, only the 20a, 2, and 20b modes are commonly observed in substituted benzenes. For the PHT neat liquid, the bands at 3084, 3061, and 3025 cm^{-1} were assigned to benzene ring modes 20a, 2, and 20b, respectively. They were in the intensity ratio of approximately 1/3.2/5.5. For the PHT SAM, the bands at 3088, 3068, and 3032 cm^{-1} were similarly assigned but the intensity ratio changed to 1/7.7/5.2. Clearly, the intensity ratio of modes 20a and 20b remained constant, but both band intensities decreased markedly with respect to mode 2 after formation of the monolayer on Au(111).

According to the infrared surface selection rule, only vibrations with transition dipole moments oriented perpendicular to the metal substrate are observed. Therefore, peak intensities are directly related to the component of each transition moment that is perpendicular to the metal surface (affected by both molecular tilt and twist angles). It should be noted that changes in the intrinsic oscillator strength, for example, by a perturbation of the vibrational potential energy surface induced by changes in layer packing, will also affect the intensity of an IR absorption band. This effect is ignored in the present discussion. The dipole moment changes associated with modes 2, 20a, and 20b are all in the plane of the phenyl ring. Simplifying the symmetry of PHT to C_{2v}, the transition dipole moment of mode 2 (a_1 symmetry) is aligned parallel and modes 20a and 20b (b_2 symmetry) are aligned perpendicular to the 1,4-axis of the benzene ring.[36−38] Because mode 2 was clearly visible in the spectrum of the PHT SAM, the phenyl 1,4-axis was not parallel to the surface plane. Furthermore, the decrease in mode 20a and 20b intensities relative to mode 2 indicated that the in-plane phenyl direction, perpendicular to the 1,4-axis, was almost parallel to the surface plane.

This conclusion was also supported by intensity changes in the aromatic C−C stretch region between 1400 and 1610 cm^{-1}. Figure 1 shows that upon formation of the PHT monolayer from the PHT solution, mode 19b (1453 cm^{-1}, b_2 symmetry) decreased relative to mode 19a (1496 cm^{-1}, a_1 symmetry).[35] It should be noted that modes 8b (b_2 symmetry) and 8a (a_1 symmetry) should also show the same effect, but interpretation was complicated because these two bands were overlapped in the spectra presented in Figure 1D.

Similar orientational arguments can be made for the VHT monolayer, but measurement of the intensities of modes 2, 20a, and 20b was complicated by the proximity of vibrational bands associated with the vinyl terminus of this molecule. The frequencies of the aromatic C−H stretching vibrations shifted to lower wavenumbers by 10−20 cm^{-1} for VHT relative to PHT because these modes involve some motion of the 1,4 position C atoms and so are sensitive to substitution at the para position.[33] Consequently, the bands at 3047 and 3018 cm^{-1} were assigned to benzene ring modes 20a and 20b in solution phase VHT. Mode 2 is strictly IR inactive for identically *p*-disubstituted benzenes,[33] so this mode was expected to be weak in all VHT spectra.

The aromatic C−C stretching modes for the VHT neat liquid were observed at approximately 1609 (8a) and 1511 cm^{-1} (19a). Unfortunately, the complementary modes 8b and 19b could not be clearly distinguished from a broad envelope of methylene modes in the 1400−1600 cm^{-1} region. It is difficult to confidently comment on the relative orientation of the phenyl group in VHT based on these bands. The out-of-plane benzene ring 17b mode appeared very distinctly at 844 cm^{-1} in the neat liquid spectrum of VHT (Figure 1A), but its counterpart was greatly diminished in the RAIR spectrum of the monolayer (Figure 1B). This observation suggests that the plane of the benzene ring adopted an orientation almost perpendicular to the gold substrate. Unfortunately, other out-of-plane modes (for example, mode 17a) that might support this hypothesis were either very weak or were obscured by features associated with the alkyl or vinyl groups of the VHT molecule.

Modes Associated with the Vinyl Group of VHT. For the VHT liquid, the terminal vinyl group gave rise to seven readily observable IR bands. The bands at 3084 and 2977 cm^{-1} can be assigned to the $=CH_2$ asymmetric ($\nu_{as}=CH_2$) and symmetric ($\nu_s=CH_2$) modes, and that at 3006 cm^{-1} is due to the vinyl C−H stretch ($\nu=CH-$). The C=C stretching vibration ($\nu C=C$) occurs at 1629 cm^{-1}, and the in-plane CH_2 deformation ($\delta=CH_2$) is at 1407 cm^{-1}. The vinyl group also has two characteristic hydrogen wag (out-of-plane) vibrations at 990 cm^{-1} ($\omega=CH-$) and 905 cm^{-1} ($\omega=CH_2$). Of significance is the difference in the ratio of peak intensities between the RAIR spectrum of the VHT monolayer and the absorbance spectrum of the liquid. The $\nu C=C$, $\delta=CH_2$, $\omega=CH-$, and $\omega=CH_2$ peaks were much less intense in the VHT monolayer spectrum, whereas the $\nu_{as}=CH_2$ and $\nu=CH-$ peaks were more intense. Because the intensities of these modes are related to the orientation of the vinyl group through the IR transition dipole moment, the approximate orientation of the vinyl moiety can be deduced. As shown schematically in Figure 2, the transition dipole moments for the $\nu C=C$ and $\delta=CH_2$ modes are parallel to the vinyl double bond, whereas that for the $\nu_{as}=CH_2$ mode is in the H−C−H plane, perpendicular to the $\nu C=C$ and $\delta=CH_2$ modes. The direction of the transition dipole moments for the out-of-plane wag modes, $\omega=CH-$ and $\omega=CH_2$, is orthogonal to the other three modes. The band intensity changes observed upon monolayer formation were consistent with an orientation in which the vinyl group double bond was almost parallel to the Au(111) plane, with the vinyl terminal H−C−H plane almost parallel to the surface normal.

3.3. STM Measurements. To obtain further information on the structure of the PHT and VHT films, STM measurements were performed. A representative large-area STM image of the PHT/Au(111) monolayer, acquired at room temperature after soaking in the PHT solution

(36) Carron, K. T.; Hurley, L. G. *J. Phys. Chem.* **1991**, *95*, 9979.
(37) Tour, J. M.; Jones, L., II; Pearson, D. L.; Lamba, J. J. S.; Burgin, T. P.; Whitesides, G. M.; Allara, D. L.; Parkh, A. N.; Atre, S. V. *J. Am. Chem. Soc.* **1995**, *117*, 9529.
(38) Wan, L. J.; Terashima, M.; Noda, H.; Osawa, M. *J. Phys. Chem. B* **2000**, *104*, 3563.

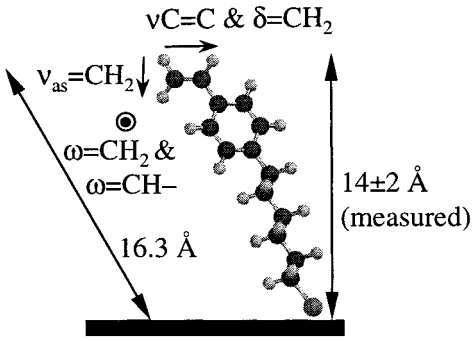

Figure 2. Schematic diagram indicating the directions of the various transition dipole moments for the vinyl group of VHT. Both the νC=C and δ=CH_2 modes are parallel to the vinyl double bond, whereas the ν_{as}=CH_2 mode is in the H−C−H plane, perpendicular to the νC=C and δ=CH_2 modes. The out-of-plane wag modes, ω=CH− and ω=CH_2, are orthogonal to the other three modes.

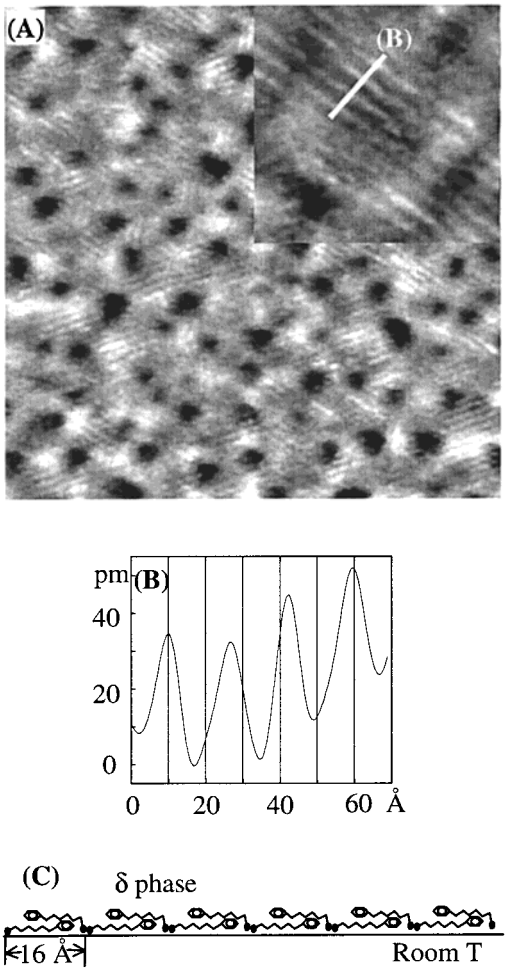

Figure 3. (A) STM images (950 × 950 Å (inset, 200 × 200 Å)) of PHT monolayers on Au/mica at room temperature show the δ stripe phase. (B) Sectional view along the line in (A) reveals the row spacing of 16 Å. (C) A schematic representation of the δ phase.

for at least 24 h, is shown in Figure 3A. The image shows many 2.5 ± 0.2 Å deep "vacancy islands". These monatomic depressions appeared to be similar in number density, size, and shape to those formed in simple alkanethiol SAMs.[39,40] Between the vacancy islands, the monolayer

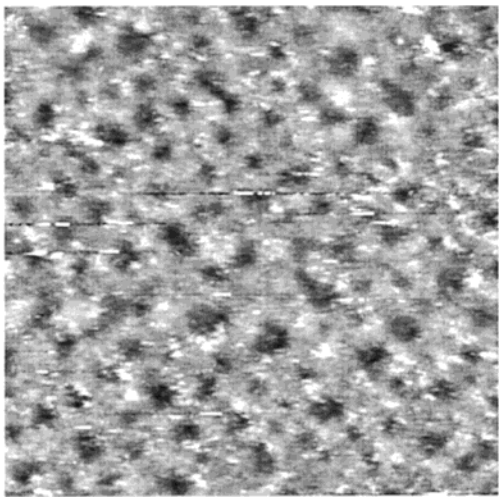

Figure 4. Typical room-temperature STM image of VHT monolayers on Au/mica (950 × 950 Å).

was composed of domains of molecular rows oriented 120 ± 5° with respect to each other. The domains appeared to be at least partially bounded by the vacancy islands. The rows in each domain had a 16 ± 1 Å corrugation period. This value is larger than the calculated single molecule length (12.6 Å) but much less than twice the molecular length. By analogy with annealed or gas-phase deposited alkanethiol films, we believe that the packing pattern adopted by the PHT film resembled the so-called δ phase of alkanethiol SAMs.[41−43] In the δ phase, the axes of one row of molecules are oriented parallel to the substrate surface, whereas a pairing row is tilted out of the surface plane, forming gauche defects near the sulfur terminus. A schematic representation is shown in Figure 3C. In this way, both S−S and alkyl−alkyl interactions are maximized. Unfortunately, at higher resolution, shown in Figure 3B, no molecular resolution was observed and the exact geometric arrangement of the phenyl−phenyl and S−S interactions cannot be determined.

A room-temperature large-area STM image of a VHT monolayer is shown in Figure 4. In common with the room-temperature PHT monolayer, it displayed monatomic deep depressions on the surface. No molecular-scale information was obtained from VHT monolayers. This failure probably resulted from disorder in the initial monolayer. As discussed previously, IR measurements suggested that at least part of the VHT molecule (the hexyl chain) was in a liquidlike environment. It was also likely that the vinyl-terminated SAM was sensitive to the tunneling current used to image the layer. As such, electron-induced reactions on the surface might contribute to the apparent poor order observed. A range of experimental tunneling conditions (tip bias from 0.7 to 3.0 V and currents down to <50 pA) were investigated, but none produced significantly improved images.

3.4. Photoreactivity of PHT and VHT Monolayers. The photoreactivity of PHT and VHT monolayers was examined by exposing them to UV light from a low-pressure Hg arc lamp for up to 45 min. Reactivity (consumption of monomer) in the VHT monolayer was observed by noting a decrease in integrated IR band intensity for all modes associated with the vinyl group, consistent with vinyl polymerization. For the PHT mono-

(39) Schönenberger, C.; Sondag-Huethorst, J. A. M.; Jorritsma, J.; Fokkink, L. G. J. *Langmuir* **1994**, *10*, 611.
(40) Poirier, G. E. *Langmuir* **1997**, *13*, 2019.
(41) Toerker, M.; Staub, R.; Fritz, T.; Schmitz-Hubsch, T.; Sellam, F.; Leo, K. *Surf. Sci.* **2000**, *445*, 100.
(42) Yamada, R.; Uosaki, K. *Langmuir* **1998**, *14*, 855.
(43) Poirier, G. E. *Langmuir* **1999**, *15*, 1167.

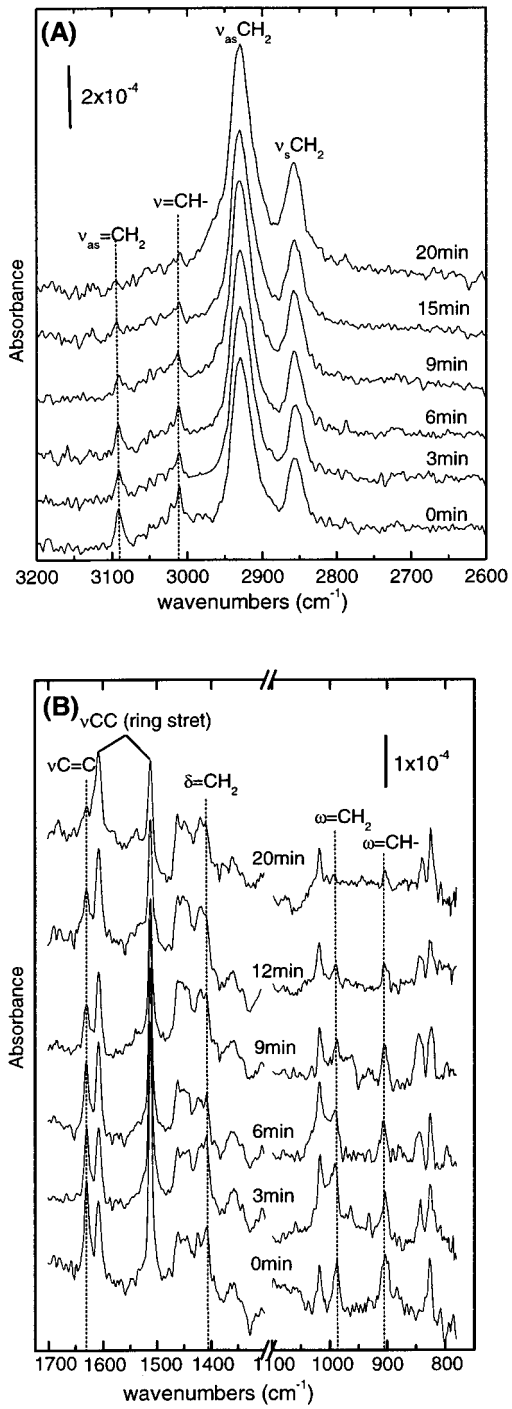

Figure 5. RAIR spectra of adsorbed VHT monolayers on Au/Si wafers obtained at various UV-light exposure times. The band intensities of various vinyl modes all decrease with increasing exposure to UV light.

layer, neither band intensities nor positions for the PHT methylene backbone and benzene ring modes changed upon UV irradiation for up to 45 min, which ensured that the spectral changes noted for VHT monolayers were due to reactions involving only the vinyl functionality.

A representative series of RAIR spectra of VHT monolayers are shown in Figure 5A,B as a function of UV exposure. The peak intensities of the vinyl modes all decreased as expected for cross-linking oligomerization reactions. During UV irradiation, intensity changes of the benzene ring modes pointed to molecular orientation changes in the VHT monolayer. The in-plane skeletal stretch at 1511 cm^{-1} (mode 19a) decreased markedly,

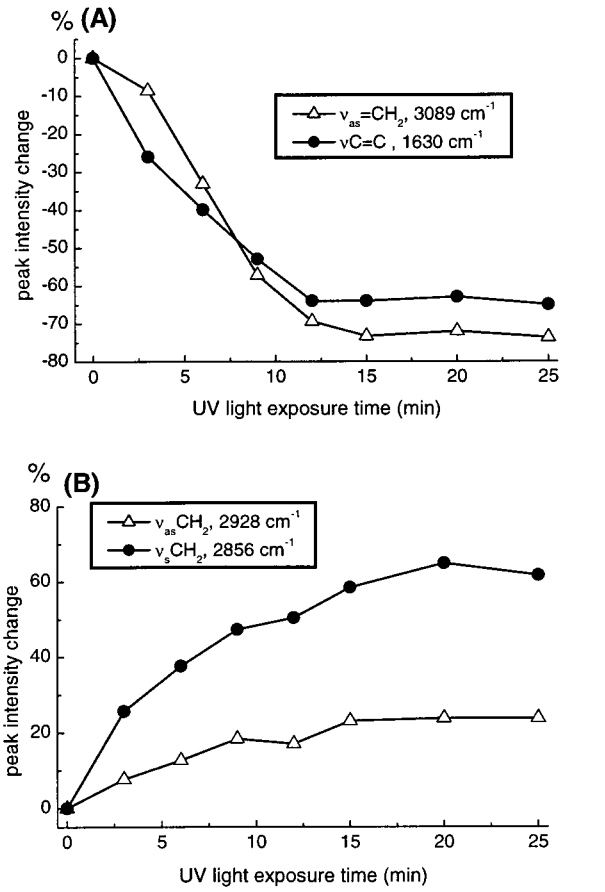

Figure 6. Plot of peak intensity change for VHT monolayers on Au/Si wafers from Figure 5 as a function of UV-light exposure time: (A) changes in the ν_{as}=CH_2 and νC=C modes and (B) changes in the $\nu_{as}CH_2$ and ν_sCH_2 modes.

implying that the phenyl ring plane became more parallel to the surface plane during VHT oligomerization (as mentioned above, no changes in phenyl mode intensities were observed during PHT monolayer irradiation). Unfortunately, additional supporting information provided by VHT mode 19b/8a/8b intensity ratios was not obtainable; mode 19b was strongly overlapped by the =CH_2 deformation, and modes 8a and 8b could not be resolved as separate features.

Confirmation that the average molecular tilt angle increased during photopolymerization of VHT monolayers was provided by pre- and post-UV exposure ellipsometry. These measurements indicated that the thickness of the film decreased from 14 ± 2 to 11 ± 1 Å following >15 min of UV irradiation. Combined with the IR intensity changes noted above, this suggests that there was some reorientation occurring within the film involving an increase in the average molecular tilt angle from ~30° to ~48° during polymerization. Similar reorientation was observed by Peanasky and McCarley following photopolymerization of undec-10-ene-1-thiol SAMs on Au.[23]

Figure 6A quantifies the absolute peak intensity change of the ν_{as}=CH_2 and νC=C modes plotted against UV exposure time. Both peak intensities decreased and reached a minimum after approximately 15 min, at which time about 30% of the vinyl bonds remained unreacted on the surface, presumably because of steric or geometric effects. No new spectral features appeared during UV irradiation. In contrast to the decreased vinyl group peak intensities, Figure 6B shows that the peak intensity for methylene ($\nu_{as}CH_2$ and ν_sCH_2) modes increased during UV irradiation. Peanasky and McCarley noted similar

effects in their study of the polymerization of undec-10-ene-1-thiol SAMs on Au by γ-ray irradiation.[23] In their work, the decrease in vinyl intensity and increase in ν_{as}-CH_2 and $\nu_s CH_2$ intensity was attributed to reaction accompanied by reorientation of the alkyl chains needed to accommodate coupling of the vinyl monomer groups. However, alkyl reorientation was not the only contribution to increased methylene intensity after oligomerization. During irradiation, the vinyl bonds reacted and new cross-linking methylene units were created. These new CH_2 groups would also contribute to an apparent increase in the intensity of the methylene bands, as observed during photopolymerization of styrene on Ag(110).[44] In conjunction with the intensity changes noted in the phenyl ring modes and the changes in monolayer thickness measured by ellipsometry, we concluded that during photopolymerization, both the new methylene units in the growing poly(styrene) chain and the orientation change of the hexyl portion of the VHT molecule contributed to the increased methylene intensity.

3.5. Thermal Stability of PHT and VHT Monolayers. The thermal stability of PHT and VHT monolayers was also tested by controlled thermal treatment in a pure N_2 environment. Upon annealing the PHT/Au(111) SAM to elevated temperatures, the vacancy islands noted at room temperature became larger and less frequent (data not shown). After heating to 60 °C, the average diameter of the depressions was 100−200 Å and contained an identical row or striped δ phase. After heating to 80 °C, as shown in Figure 7A, the vacancy islands disappeared and the surface was completely covered by parallel rows of features oriented at approximately 120° with respect to each other. The domains were much larger than at room temperature and were terminated by sharp boundaries. Again, by analogy with the phases observed for annealed alkanethiols on Au(111), we assigned this structure as the χ' phase,[41] shown schematically in Figure 7C. In our PHT SAM, the χ' phase was characterized by parallel stripes, randomly separated by either 16 ± 1 or 28 ± 1 Å. We attributed the 16 Å stripe spacing as a similar structure to the δ phase. We believed that the 28 Å spacing (which is almost exactly twice the calculated molecular length plus a S−S distance of 4 Å[41]) was due to alternating head-to-head and tail-to-tail molecules arranged with their molecular axes almost parallel to the surface plane. An interesting feature of this phase was that the distance between rows was observed to switch from 28 to 16 Å, or vice versa, at random places along the row, as shown in Figure 7B. A plausible explanation for this phenomenon involves the expansion of a 16 Å row or compression of a 28 Å row, followed by the lateral shift of the entire stripe segment as proposed by Toerker et al. for decanethiol phases on Au(111).[41]

The χ' phase appeared to be an intermediate state between the δ phase and β phase observed at higher annealing temperatures. After the formation of the χ' state, the continued annealing of PHT monolayers on Au(111) resulted in surfaces covered with the β phase in which all the molecular axes were parallel to the substrate surface plane with sulfur atoms paired and chains packed head-to-head and tail-to-tail, as shown schematically in Figure 8C. After annealing to 120 °C, as shown in Figure 8A, large single domains of striped β phase characterized by a row separation of 28 ± 1 Å were visible. The ordered regions of the monolayer contained a few short sections of the narrow δ phase rows as illustrated in Figure 8B. Additionally, significant fractions of the surface were covered by a disordered or mobile liquidlike phase, visible in the lower right-hand corner of Figure 8A.

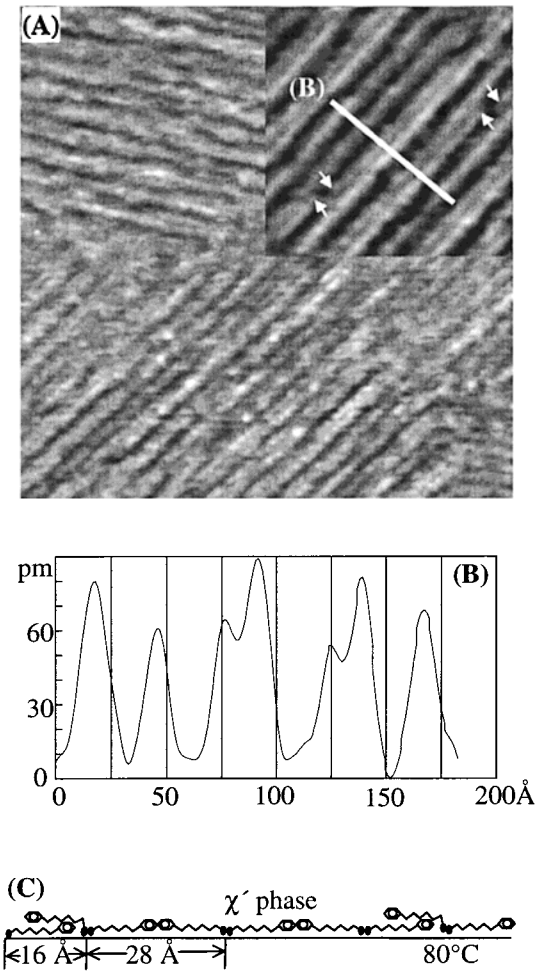

Figure 7. (A) STM images (800 × 800 Å (inset, 250 × 250 Å)) of PHT monolayers on Au/mica at 80 °C show the χ' stripe phase. The arrows indicate the switching of stripe segments. (B) Sectional view along the line in (A) reveals the row spacing of either 16 or 28 Å. (C) A schematic representation of the χ' phase.

We also acquired STM images of VHT monolayers annealed up to 120 °C (not shown). The images were qualitatively very similar to Figure 4 at all temperatures. Significantly, at no time did we observe evidence of row or stripe phases typically observed for annealed conventional alkanethiols and indicative of a reduced surface coverage.[41] The increased stability of the VHT monolayer versus the PHT monolayer probably resulted from the thermal polymerization discussed below.

Figure 9 shows the 2700−3200 cm^{-1} region RAIR spectra of an unpolymerized VHT monolayer as a function of annealing temperature.[45] The peak intensity of all modes associated with the vinyl bond decreased with increasing temperature; the ν_{as}=CH_2 mode had effectively disappeared after annealing to 130 °C. Concurrently, a new feature at 2964 cm^{-1} attributed to $\nu_{as}CH_3$ grew in as the annealing temperature increased. The appearance of the methyl mode was evidence that a fraction of the vinyl bonds opened during heating became terminated with CH_3 end groups. It should be stressed that no methyl features appeared in the case of VHT *photo*polymerization (shown

(44) Carlo, S. R.; Grassian, V. H. *Langmuir* **1997**, *13*, 2307.

(45) During annealing, the sample was heated at approximately 3 °C/min to the indicated temperature and immediately cooled to room temperature. The average cooling rate was approximately 5−8 °C/min.

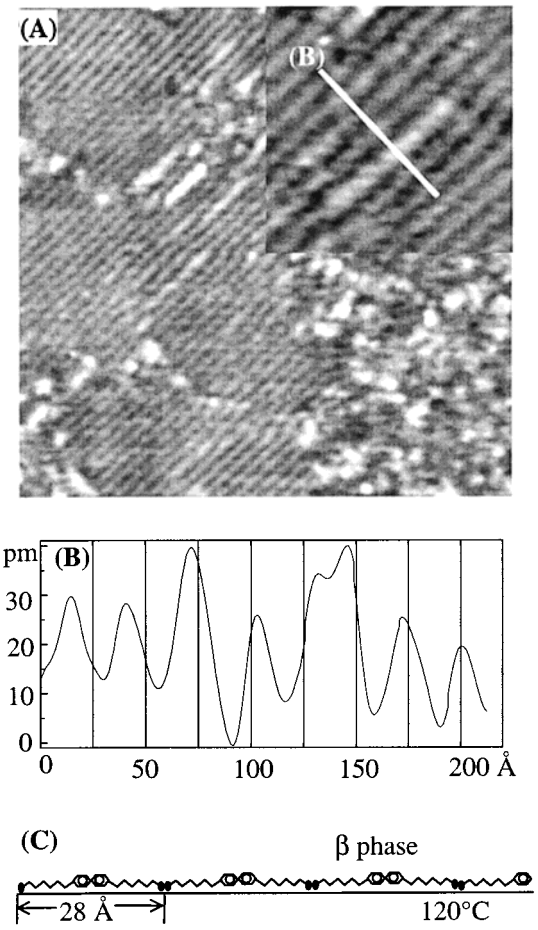

Figure 8. (A) STM images (1000 × 1000 Å (inset, 250 × 250 Å)) of PHT monolayers on Au/mica at 120 °C show the β stripe phase. (B) Sectional view along the line in (A) reveals the row spacing of 28 Å. (C) A schematic representation of the β phase.

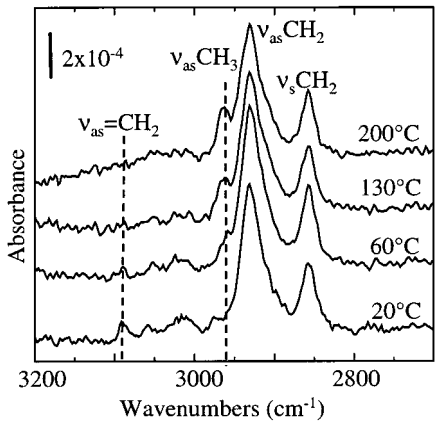

Figure 9. RAIR spectra of adsorbed VHT monolayers on Au/Si wafers obtained following annealing at the indicated temperature.

in Figure 5A), even after extended UV irradiation times. Although we cannot quantitate the degree of polymerization for the thermal and photopolymerized monolayers, it seems clear that thermal activation produced shorter oligomers with a larger number of terminal methyl groups.

Figure 10 shows the effect of annealing on a prephotopolymerized VHT monolayer (15 min UV irradiation). The data are similar to those in Figure 9, but the initial intensity of the vinyl group ν_{as}=CH_2 mode at 3089 cm^{-1} was much reduced (approximately 30% of the vinyl bonds remained intact after photopolymerization). Annealing

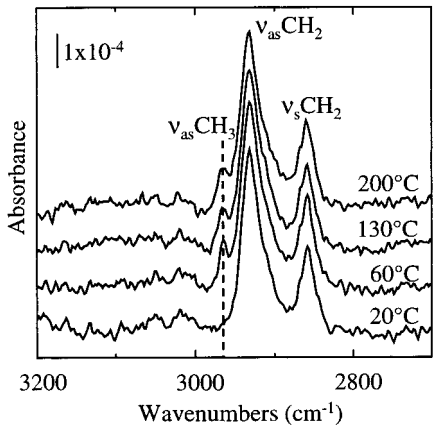

Figure 10. RAIR spectra of prephotopolymerized VHT monolayers on Au/Si wafers obtained following annealing at the indicated temperature.

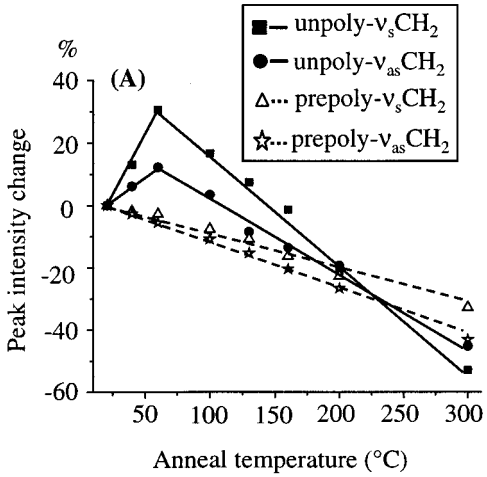

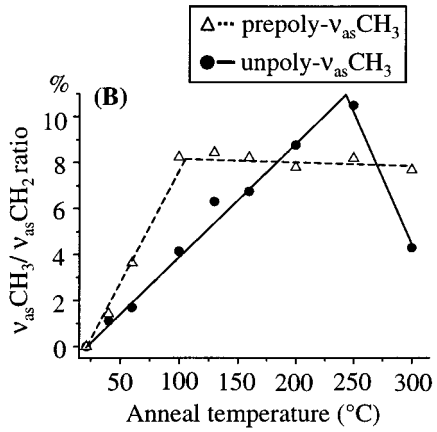

Figure 11. Plot of peak intensity change for unpolymerized and prephotopolymerized VHT monolayers on Au/Si wafers from Figures 9 and 10 as a function of annealing temperature: (A) changes in the $\nu_{as}CH_2$ and ν_sCH_2 modes and (B) changes in the $\nu_{as}CH_3$ mode (shown as the ratio of $\nu_{as}CH_3$ peak intensity divided by that of the initial unpolymerized $\nu_{as}CH_2$ mode).

of the prephotopolymerized monolayer also resulted in the appearance of a feature assignable to methyl ($\nu_{as}CH_3$ at 2964 cm^{-1}) but at a slower rate than for the unpolymerized VHT film.

The integrated peak areas for the methylene ν_s and ν_{as} modes of the prephotopolymerized and unpolymerized VHT monolayers are shown in Figure 11A as a function of annealing temperature. For the unpolymerized monolayer, both $\nu_{as}CH_2$ and ν_sCH_2 modes increased up to 60 °C,

but the $\nu_s CH_2$ mode increased faster than the $\nu_{as} CH_2$ mode. Such behavior was also observed during the photopolymerization experiments, as discussed previously, and attributed to growing poly(styrene) oligomers together with orientational effects in the underlying molecule. We believe the growth of the $\nu_{as} CH_2$ and $\nu_s CH_2$ modes during thermal treatment was also related to oligomerization reactions within the monolayer. However, the absolute increase of both modes was less than that of the photopolymerized film. Ellipsometry indicated that the film thickness also decreased by 3 ± 1 Å during annealing, identical to the decrease observed during photopolymerization. If we assumed that the hexyl chain orientation change was similar for both thermal and photopolymerization, the less rapid increase of the $\nu_{as} CH_2$ and $\nu_s CH_2$ modes during thermal polymerization indicated a lower average degree of polymerization. As discussed above, the increased ν_{as}-CH_3 mode intensity with annealing supported the idea that the polymers formed by thermal annealing were short-chain oligomers with CH_3 end groups. Decomposition of the thermally polymerized monolayer above 60 °C was signaled by rapid decreases in both methylene modes and a continuous increase in the $\nu_{as} CH_3$ mode up to 250 °C, as shown in Figure 11B. The appearance of methyl vibrational modes implied cleavage of the poly(styrene) chains.

For the prephotopolymerized monolayer, as shown in Figure 11A, both $\nu_{as} CH_2$ and $\nu_s CH_2$ modes decreased monotonically with increasing annealing temperature. The rate of decrease of these modes was much less rapid than for the unpolymerized film (above 60 °C), suggesting that the prephotopolymerized film had increased thermal stability. It will be recalled that the prephotopolymerized film contained about 30% unreacted vinyl groups at the start of the annealing process. These bonds appeared to be thermally activated to produce methyl groups upon annealing up to 100 °C, as signaled by a rapid rise in the $\nu_{as} CH_3/\nu_{as} CH_2$ intensity ratio shown in Figure 11B. For all temperatures above 100 °C, this ratio remained constant, likely because of the consumption of all reactive vinyl groups.

The compositional differences between the thermally polymerized and photopolymerized VHT SAMs were striking. Thermal polymerization produced a significant number of CH_3 groups, whereas these functionalities were almost completely absent for the photopolymerized monolayer. We believe that the most probable cause of these differences was related to additional molecular motion present in the VHT monolayer at elevated temperatures. Increased motion created a wide range of potential reaction geometries and, in turn, a reduced specificity for successful cross-linking. There appeared to be no significant change in the degree of order or gross structure of the VHT SAM during annealing, as evidenced by the constant width and position of the methylene ν_s or ν_{as} bands and by the ellipsometric thickness changes (an identical decrease in film thickness was observed for both thermo- and photopolymerized VHT SAMs). We can therefore tentatively discounted the formation of a discrete high-temperature phase with a structure not conducive to cross-linking as the cause of a reduced degree of polymerization during thermal versus photochemical polymerization.

4. Conclusions

The self-assembly of mixed aliphatic/aromatic thiols 6-phenyl-*n*-hexanethiol and 6-(*p*-vinylphenyl)-*n*-hexanethiol on Au(111) has been investigated. We have characterized both SAMs by RAIR spectroscopy, ellipsometry, and STM. The RAIR spectral data indicated that both molecules chemisorbed on gold as thiolates; however, the alkyl chains were disordered for both SAMs. Ellipsometry and infrared measurements suggested that the PHT monolayer had an average molecular axis close to parallel to the surface plane. Scanning tunneling microscopy revealed that the PHT SAM was composed of small domains of molecules arranged in rows. The average corrugation of the rows was 16 ± 1 Å, consistent with a so-called δ phase by analogy with the structures of simple alkanethiol SAMs. We investigated the structural changes of the PHT monolayer with annealing in ultrahigh vacuum, and three different stripe phases (δ, χ', and β) were observed by STM. All three phases were characterized by alignment of the molecular axes with the surface plane.

In contrast, the VHT monolayer had a structure in which the average molecular tilt angle was close to the surface normal. As with the azobenzene derivative SAMs,[16−20] a small modification of the molecular structure (from PHT to VHT) changes the monolayer morphology completely. In our case, this effect could be simply related to the presence of an additional two C atoms in the case of VHT stabilizing the "standing up" orientation (as observed for hexanethiol versus octanethiol, on Au(111), for example). However, the disordered nature of the alkyl tethers of both PHT and VHT monolayers implied that aliphatic stabilizing interactions did not completely dominate film morphology. The involvement of styrene−styrene contributions to the molecular orientation in styrene-containing SAMs can also be inferred from the standing up orientation deduced for much shorter *p*-alkyl styrene monolayers ((mercaptomethyl)styrene).[22]

Like the PHT SAM, the room-temperature VHT SAM exhibited monatomic depressions (vacancy islands) as imaged by STM, but further details could not be resolved. Polymerization of the VHT SAM, as followed by RAIRS, was achieved by either UV-light irradiation or thermal treatment. We speculated that UV irradiation produced longer chain polymers up to a maximum of ∼70% conversion. In contrast, thermal annealing produced shorter chain polymers with a large proportion of CH_3 end groups. The UV-light polymerized film was more robust to degradation than the thermally polymerized film.

Acknowledgment. We gratefully acknowledge Professor G. L. Baker and Jong-Bum Kim for assistance with the synthesis of PHT and VHT. We thank Professor M. L. Bruening for his help with FTIR data acquisition and many helpful discussions. This work was partly supported by the Center for Fundamental Material Research (CFMR) at Michigan State University.

LA001633U